

An optoelectronic heterostructure for neuromorphic computing: CdS/V3O5

C Adda, H Navarro, J Kaur, M-H Lee, C Chen, M Rozenberg, S P Ong, Ivan K Schuller

▶ **To cite this version:**

C Adda, H Navarro, J Kaur, M-H Lee, C Chen, et al.. An optoelectronic heterostructure for neuromorphic computing: CdS/V3O5. Applied Physics Letters, 2022, 121 (4), pp.041901. 10.1063/5.0103650 . hal-03854113

HAL Id: hal-03854113
https://hal.science/hal-03854113

Submitted on 15 Nov 2022

HAL is a multi-disciplinary open access archive for the deposit and dissemination of scientific research documents, whether they are published or not. The documents may come from teaching and research institutions in France or abroad, or from public or private research centers.

L'archive ouverte pluridisciplinaire **HAL**, est destinée au dépôt et à la diffusion de documents scientifiques de niveau recherche, publiés ou non, émanant des établissements d'enseignement et de recherche français ou étrangers, des laboratoires publics ou privés.

Applied Physics Letters

An optoelectronic heterostructure for neuromorphic computing: CdS/V_3O_5

Cite as: Appl. Phys. Lett. **121**, 041901 (2022); https://doi.org/10.1063/5.0103650
Submitted: 16 June 2022 • Accepted: 13 July 2022 • Published Online: 28 July 2022

C. Adda, H. Navarro, J. Kaur, et al.

View Online Export Citation CrossMark

QBLOX



1 qubit

Shorten Setup Time
Auto-Calibration
More Qubits

Fully-integrated
Quantum Control Stacks
Ultrastable DC to 18.5 GHz
Synchronized <<1 ns
Ultralow noise



100s qubits

visit our website >

© 2022 Author(s).

Applied Physics Letters ARTICLE scitation.org/journal/apl

An optoelectronic heterostructure for neuromorphic computing: CdS/V_3O_5

Cite as: Appl. Phys. Lett. **121**, 041901 (2022); doi: 10.1063/5.0103650
Submitted: 16 June 2022 · Accepted: 13 July 2022 ·
Published Online: 28 July 2022

View Online Export Citation CrossMark

C. Adda,[1,a] H. Navarro,[1,a] J. Kaur,[2,3] M.-H. Lee,[1] C. Chen,[2] M. Rozenberg,[4] S. P. Ong,[2] and Ivan K. Schuller[1]

AFFILIATIONS

[1]Department of Physics and Center for Advanced Nanoscience, University of California San Diego, La Jolla, California 92093, USA
[2]NanoEngineering Department, University of California San Diego, La Jolla, California 92093, USA
[3]Materials Science and Engineering Program, University of California San Diego, La Jolla, California 92093, USA
[4]Université Paris-Saclay, CNRS, Laboratoire de Physique des Solides, 91405 Orsay, France

[a)]**Authors to whom correspondence should be addressed:** hnavarro@physics.ucsd.edu and cadda@physics.ucsd.edu

ABSTRACT

Nonvolatile resistive switching is one of the key phenomena for emerging applications in optoelectronics and neuromorphic computing. In most of the cases, an electric field is applied to a two terminal dielectric material device and leads to the formation of a low resistance filament due to ion migration. However, the stochastic nature of the ion migration can be an impediment for the device robustness and controllability, with uncontrolled variations of high and low resistance states or threshold voltages. Here, we report an optically induced resistive switching based on a CdS/V_3O_5 heterostructure which can overcome this issue. V_3O_5 is known to have a second order insulator to metal transition around $T_c \approx 415$ K, with an electrically induced threshold switching at room temperature. Upon illumination, the direct transfer of the photoinduced carriers from the CdS into V_3O_5 produces a nonvolatile resistive switching at room temperature. The initial high resistance can be recovered by reaching the high temperature metallic phase, i.e., temperatures above T_c. Interestingly, this resistive switching becomes volatile around the T_c. By locally manipulating the volatile and nonvolatile resistive switching using electric field and light, this system is a promising platform for hardware based neuromorphic computing implementations.

Published under an exclusive license by AIP Publishing. https://doi.org/10.1063/5.0103650

Resistive switching is a very active research field and is developing rapidly due to its fundamental interest and potential applications, such as nonvolatile resistive random-access memories (RRAM),[1] memristors,[2] or neuromorphic computing.[3–6] This phenomenon mostly refers to an electric field induced reversible, nonvolatile resistive switching of a dielectric material (like a transition-metal oxide) sandwiched between two electrodes. Under a voltage pulse (SET mechanism), the two-terminal device switches from a high resistance state (HRS) to a low resistance state (LRS) and remains in the LRS. The physical mechanism behind the resistive switching is generally ion migration forming oxygen-vacancy or metal-atom filaments bridging the electrodes.[7] Successive electric field pulses can dissolve the filaments (RESET mechanism), bringing the device back to a HRS. On the other hand, strongly correlated materials, such as temperature-driven insulator to metal transition (IMT) compounds,[8] can also exhibit an electrically induced resistive switching below the transition temperature (T_c). The most studied compounds are VO_2 and V_2O_3. In these cases, the resistive switching is volatile (also called threshold switching) since the resistance of the material returns to its initial value once the electrical bias is removed. In contrast to the previous nonvolatile effect that involved ionic migration, it has been demonstrated on several IMT materials that this volatile resistive switching is a result of the formation of a voltage induced metallic filament.[9,10] In addition, it was shown that the nonvolatile resistive switching could be induced in VO_2 devices far from T_c, leading to the creation of a new vanadium oxide phase filament.[11] So far, the electrically triggered resistive switching has been extensively studied in these strongly correlated materials. On the other hand, different optoelectronic resistive switching systems have been reported, where light induces threshold switching,[12,13] enhances or modulates resistive switching and threshold switching,[14–18] or the resistive switching is volatile.[19] The optical control of the switching response has attracted much attention over the past few years.

Recently, we have shown that combining an ultra-thin film (10 nm) of V_2O_3 or VO_2 with a photoresistor cadmium sulfide (CdS) layer allows for a modulation of the transition temperature and the resistance in the low temperature insulating phase upon visible light.[20] CdS is a semiconductor that generates a high concentration of charge

Published under an exclusive license by AIP Publishing

carriers (holes and electrons) when exposed to light.[21] In the previous work,[20] it was reported that illumination of a CdS/V_2O_3 heterostructure, under illumination of the transition, completely suppresses the transition, leading to a giant resistance decrease in at least six orders of magnitude. In the CdS/VO_2 case, the resistance change was smaller but still remarkable, and the transition was not completely suppressed but shifted to lower temperatures by ∼15 K. The resistance modulation was volatile in the CdS/V_2O_3, i.e., it recovered its initial resistance when the illumination is stopped. However, the modulation is essentially nonvolatile in the case of the CdS/VO_2 heterostructure, i.e., the change in resistance $R(T)$ under illumination remained the same after the illumination was removed. However, after 8 h at 300 K, the heterostructure recovered its initial $R(T)$, thus reversing the modulation effect. Therefore, the switching mechanism may be different between different CdS/oxides systems.

In this work, we focus on another vanadium oxide, V_3O_5, which, in contrast to VO_2 and V_2O_3, exhibits a second order IMT around $T_c \approx 415$ K. Here, we sputtered a CdS layer on top of a V_3O_5 thin film, and we studied the effect of the light on the resistance of this heterostructure. Our results show a nonvolatile resistive switching at room temperature upon illumination, i.e., 120 K below T_c. The resistive switching ratio is about 80%. As the temperature increases, the resistive switching ratio decreases (down to 32%), and the switching becomes volatile. Density-functional theory (DFT) calculations show that localization of trapped electron in naturally present oxygen vacancies is responsible for the nonvolatile resistive switching. Contrary to VO_2 that does not relax even at high temperature, in the V_3O_5, the resistance returns to its initial state once the temperature is above T_c. As shown previously,[22] the V_3O_5 high temperature phase can be reached by electrically triggering volatile resistive switching. Our results provide, therefore, a great platform for neuromorphic computing applications, especially using electrically induced switching. In addition, because in our structure, no ion migration is involved, these heterostructures overcome robustness and controllability issues arising from ion migration. Thus, CdS/V_3O_5 devices could be used to implement neuron-like (electrical bias) and synapse-like (light + electrical bias) functionalities in the same material system.

Figure 1(a) shows the changes in the resistance vs temperature [$R(T)$] when illuminating the CdS/V_3O_5 hybrid [Fig. 1(a)] compared to $R(T)$ in the dark. Without illumination [black (heating 1—cooling 2)] curves in Fig. 1(a), the CdS/V_3O_5 hybrid exhibits a second order IMT around 415 K, as expected.[23,24] This $R(T)$ curve is similar to previous studies[22,25] with a strong nonlinear temperature dependence within the insulating state (300–400 K) and a change of resistance during the phase transition (factor of 3 between 400 and 420 K). The illumination of the CdS/V_3O_5 hybrid with a white LED induces a resistive switching at room temperature of a factor of 5. A clear resistive switching can be observed when comparing the initial $R(T)$ measured in the dark, with the $R(T)$ measured upon a 481 mW/cm^2 illumination at 300 K [black (heating 1—cooling 2) and orange (heating 3—cooling 4) curves, respectively]. We note that the resistance changes decrease with increasing the temperature. Illumination of a bare V_3O_5 thin film with the same power density shows no resistance variations, implying that this phenomenon is not caused by thermal heating. Interestingly, in VO_2,[18] the resistance change remains during both heating and cooling curves in the illuminated state even after switching off the light. On the other hand, the resistance of V_3O_5 increases slightly in the dark but does recover its original value around the phase transition temperature (dashed blue line—heating curve 5). The initial state is recovered in the cooling loop (dashed blue line—cooling curve 6). Therefore, in the CdS/V_3O_5 hybrid, illumination provides a SET mechanism, and the voltage induced transition into in the high temperature phase would provide the RESET mechanism.

The CdS/V_3O_5 hybrid shows strong resistive switching when illuminated. Figure 1(b) shows the time dependence of the resistance normalized to the insulating pristine state (before illumination) at 300 K. At $t = 0$, the light is switched on, illuminating the hybrid with a 481 mW/cm^2 power density. The resistance of the V_3O_5 (R/R_{dark})

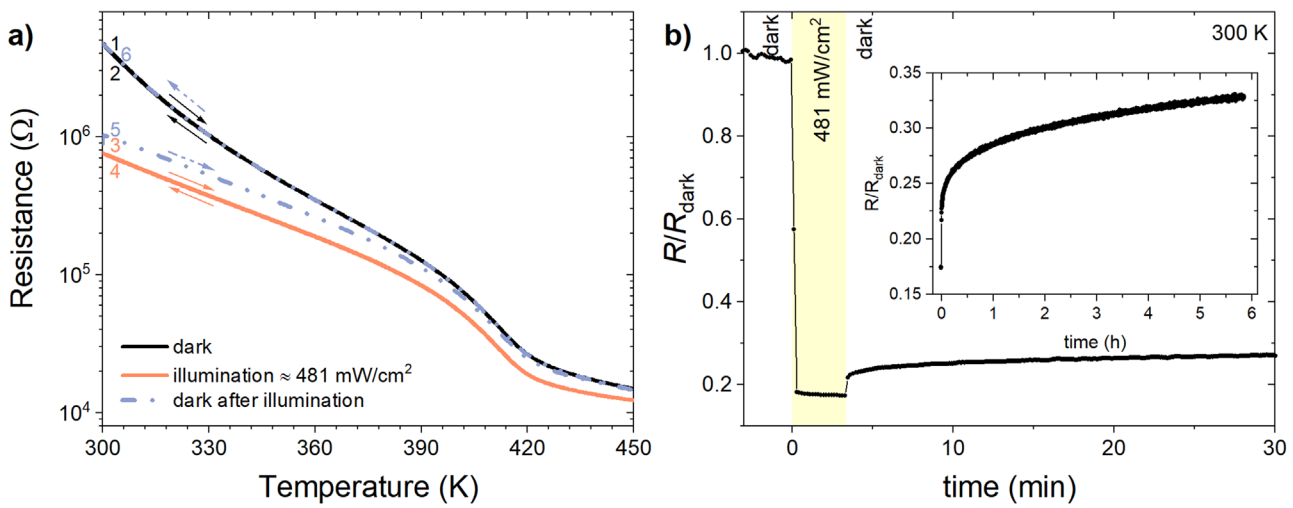


FIG. 1. (a) Resistance of CdS/V_3O_5 hybrid as a function of temperature. Black and orange curves correspond to the dark and 481 mW/cm^2 illumination, respectively. Dashed curves (5 and 6) obtained after illumination. Arrows indicate sweep directions. (b) Time dependence of the same hybrid at 300 K. The resistance normalized to before illumination. At $t = 0$, 481 mW/cm^2 illumination started that abruptly changes the resistance by a factor of 5 until turned off at $t \approx 3$ min. The inset shows resistance relaxation for 6 h.

Published under an exclusive license by AIP Publishing

abruptly changes by a factor of 5. After removing the light, the resistance slightly increases but remains in a low resistance value. Our measurement shows that after 6 h, the V_3O_5 only recovered 32% of its initial state, i.e., the relaxation of the resistive switching ratio [$\Delta R = (R_{dark} - R_{ill})/R_{dark}$] is around 17%. A direct measurement of the full recovery time is too long to be feasible. From a fit of the short time recovery of the resistance (see the supplementary material), we estimate that a 50% recovery of the initial resistance would take more than 10 years. So, in order to accelerate the time to recover R_{dark}, the heterostructures are heated above T_c.

Figure 2(a) shows the time dependence of the normalized resistance change at different temperatures. The amplitude and the nature (volatile vs nonvolatile) of the resistive switching are strongly dependent on the temperature. For temperatures below T_c (< 400 K), the resistive switching ratio (ΔR) decreases with increasing the temperature [Fig. 2(c)]. At 400 K (near T_c), however, the resistive switching ratio becomes non-monotonic and is more pronounced than at 360 and 380 K, suggesting a change of regime near the onset of the phase transition. The relaxation of the resistance after illumination [Fig. 2(b)] fits well to a stretched exponential as shown in the supplementary material. Far below the phase transition, the resistive switching is "non-volatile," i.e., the resistance relaxes only slightly. 1 h after the LED was turned OFF, the resistance ratio only relaxed by 10% [Fig. 2(c)]. We found that the higher the temperature, the smaller the nonvolatility effect of the resistive switching. The V_3O_5 has, indeed, relaxed by 39% of its initial resistance at 340 K, 56% at 360 K, 72% at 380 K, and 89% at 400 K. Hence, the resistive switching that is nonvolatile at room temperature becomes volatile at higher temperature, just beneath the onset of the phase transition.

To elucidate the photoinduced effect, we performed DFT calculations to understand the defects present in V_3O_5 and the effects of electron doping. We find that oxygen vacancies are the most stable defects in the case of LT (low temperature) phase (Fig. S1), which has also been reported experimentally by Rua *et al.*[26] The methods used for the defect calculations are presented in the supplementary material, and the various defect energies as a function of oxygen chemical potential are shown in Fig. S1.

DFT calculations were performed on supercells with negatively charged oxygen vacancies with varying electron density. We note that for computational tractability, the calculations utilized a single oxygen vacancy within a 2 × 2 × 2 supercell (96 formula units), which significantly overestimates the density of oxygen vacancies. Nevertheless, we expect that the qualitative trends are still valid. With a charged oxygen vacancy, the bandgap decreases from 0.63 to 0.40 eV [Figs. 3(e) and 3(f); a wider DOS is shown in the supplementary material]. The Density of State (DOS) for the system with negatively charged oxygen vacancies reveals the appearance of a small peak near E_F, in the forbidden zone [Fig. 3(f)]. This suggests a deep state with electron localization. The localization can be further confirmed from the atomic DOS for vanadium sites present in the near vicinity of the oxygen vacant site, where the same small peak is observed near the E_F (Fig. S2). The same phenomenon can also be observed from the wavefunction plots in Fig. S3(c). This peak vanishes for vanadium sites further away from the oxygen vacancy. We note that this localization is observed only with negatively charged oxygen vacancies, indicating no possibility of hole doping in the system. Figure S5 shows that the hole doped system is metallic as the E_F is inside the valence band. Moreover, the presence of small peak just below the E_F confirms that the electrons (generated by CdS under illumination) are injected in V_3O_5 and are trapped into this deep state, slowing the "low" temperature relaxation rate. For the LT phase ($T < 340$ K), the photoexcited electrons trapped into the oxygen vacancy are unable to overcome the barrier, and therefore, no relaxation is observed. At higher temperatures, relaxation is induced by thermal excitation of the trapped electron over the barrier and via the thermally accessible conduction band.

The above results imply that the nonvolatile resistive switching is due to charge-transfer of the photoinduced carrier.[27,28] The photon absorbed in the CdS excites an electron into the conduction band, and this has a finite probability to be transferred into the V_3O_5. The electron doping in oxygen-deficient V_3O_5 produces a decrease in the resistance by decreasing the gap as well as filling the in-gap state produced by the oxygen vacancies [Fig. 3(b)]. Illumination decreases the Fermi level. Although some carriers in the higher in-gap states may thermally relax, most of the carrier remain trapped in the in-gap state, unable to

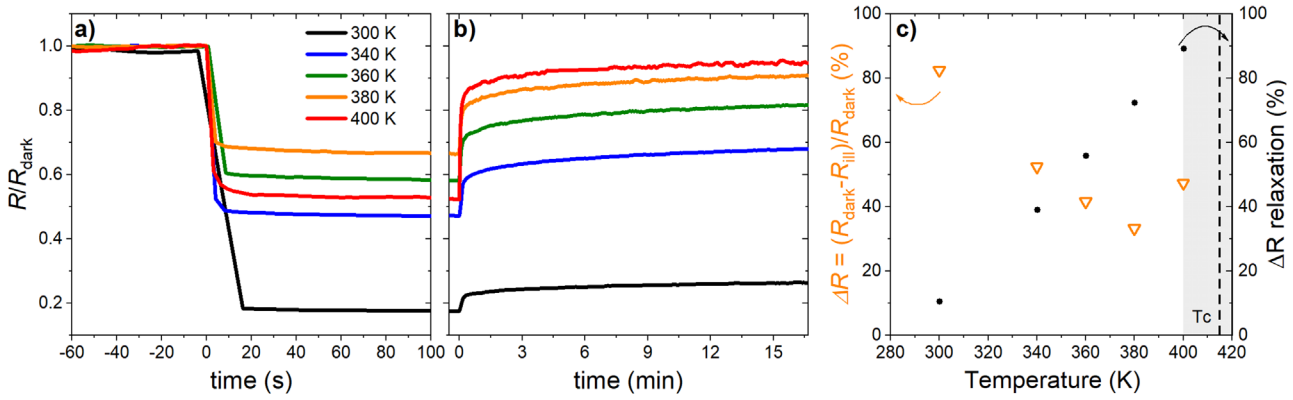


FIG. 2. (a) Time dependence of the resistance normalized to the insulating state at different temperatures. At $t = 0$, the sample is illuminated, and the system switches into a low resistance state. (b) Time dependence of the resistance normalized to the insulating state. At $t = 0$, the LED is switched OFF. (c) Temperature dependence of resistive switching ratio ($\Delta R = (R_{dark} - R_{ill})/R_{dark}$) (orange triangle) and relaxation of ΔR (ΔR *relaxation* $= (\Delta R - \Delta R_{after\ illumination})/\Delta R$) (black dots) after 1 h.

Published under an exclusive license by AIP Publishing

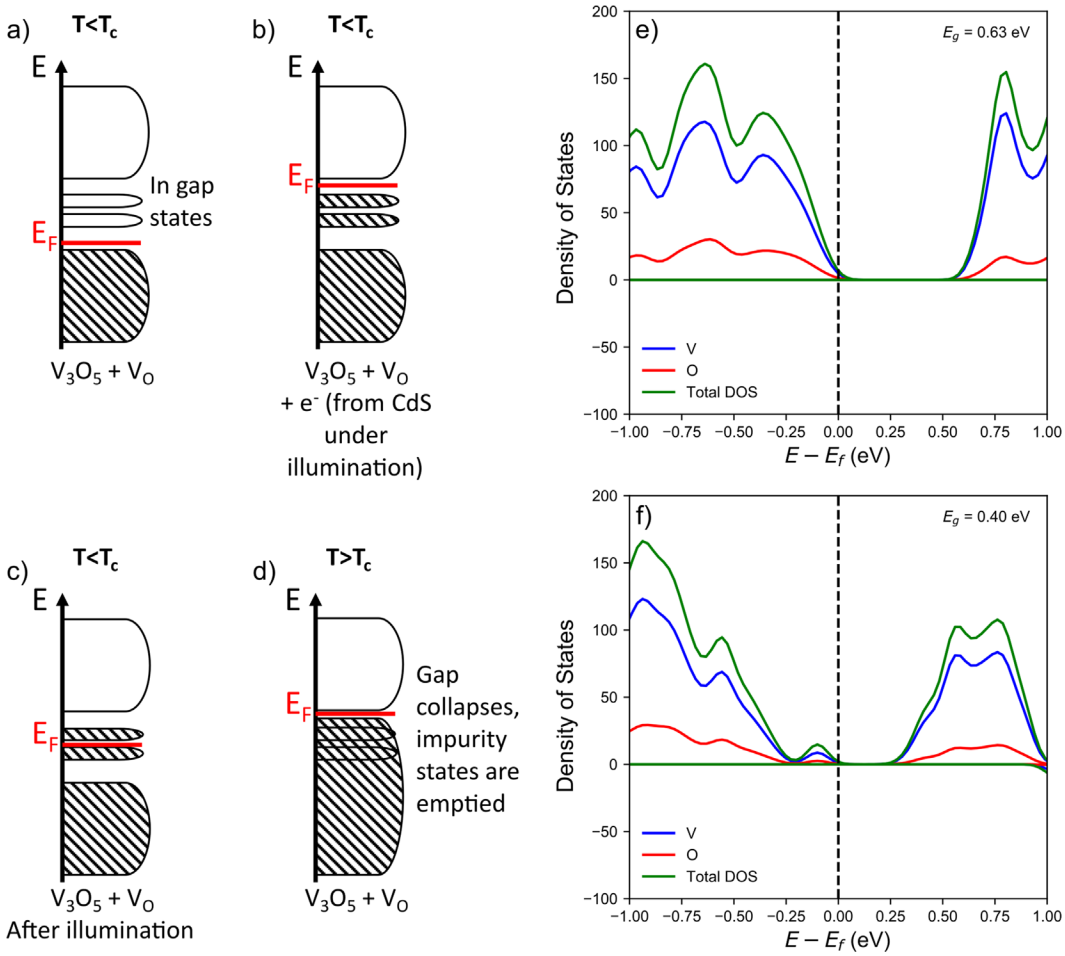


FIG. 3. (a)–(d) Schematics proposed mechanism for the nonvolatile resistive switching in the CdS/V_3O_5 hybrid. (a) Band structure of V_3O_5 with in-gap state due to the presence of oxygen vacancies. (b) Under illumination, electrons from CdS are doping the V_3O_5, and filling the oxygen vacancies in gap state. (c) Once the illumination is removed, the system is no longer doped but remains in the low resistance state since electrons are trapped in oxygen vacancies. (d) At temperatures above T_c, the gap thermally closes, and electrons trapped into the oxygen vacancies are released. The system then goes back to the case a), where the Fermi level is low and far from the conduction band. (e) and (f) Total (green), O-2p (red), and V-3d (blue) orbital density of states (DOS) for a $2 \times 2 \times 2$ supercell of (e) LT stoichiometric V_3O_5 and (f) nonstoichiometric V_3O_5 containing a negatively charged oxygen vacancy. A decrease in the bandgap can be seen from 0.63 eV in (e) to 0.40 eV in (f).

overcome the energy barrier. As a consequence, the system remains in the low resistance state [Fig. 3(c)]. At higher temperature, when reaching the phase transition, the gap is thermally closing, and the thermal excitation is more important. This results in the relaxation of trapped carrier, either by thermal excitation or via the thermally accessible conductions bands.

In conclusion, we have demonstrated illumination induced room temperature nonvolatile resistive switching in a CdS/V_3O_5 heterostructure. This light-induced resistive switching can be reset at higher temperature at $T > 415$ K. Although the resistive switching is nonvolatile at temperatures far below T_c, it becomes volatile when close to the transition ($T > 380$ K). The relaxation of the resistance after illumination has been fitted with stretch exponentials, and the extracted thermally activated relaxation times correspond to an energy barrier close to 847 meV. Contrary to the common electrically induced filamentary resistive switching observed in many simple oxides, the resistive switching presented here is due to photodoping, with carriers created in the CdS during the illumination and injected into the V_3O_5. DFT calculations support the idea that photoexcited electrons can be trapped into oxygen vacancies and are unable to overcome the energy barrier at room temperature. Moreover, this non-volatility could be incorporated with volatile resistive switching (threshold switching)[22] in simple V_3O_5 two-terminal device based systems. The neuron-like functionalities could be emulated by electrical excitation, and the coupling of light (SET) and electrical (RESET) excitations would lead to synapse-like functions. This opens the use of a new optoelectronic type memristor for emergent neuromorphic computing.

The V_3O_5 film was synthetized by transforming a V_2O_3 (60 nm) film grown on $\langle 012 \rangle$ Al_2O_3 through a gas evolution technique.[25] This system allows for precise control of the oxygen partial pressure and temperature starting from high vacuum conditions. A thorough description of this technique and a detailed investigation of the

Published under an exclusive license by AIP Publishing

electrical, structural, and compositional properties of the V_3O_5 thin film can be found in our previous paper.[25] The sample was annealed at 837 °C under an oxygen partial pressure $\sim 9 \times 10^{-8}$ Torr for 6 h, until the oxidation from V_2O_3 into V_3O_5 was complete. θ–2θ XRD and reciprocal space maps together with a sharp metal-insulator transition indicate the presence of single phase V_3O_5 thin films after annealing. On top of these films, we deposited an 80 nm thick CdS film using rf magnetron sputtering, in a 2-mTorr pure argon atmosphere at 180 °C. Two 500 μm wide electrodes were pattern in a coplanar geometry and were separated with a 6 mm distance on top of the CdS/V_3O_5 heterostructures. XRD measurements were performed in a Rigaku SmartLab system at room temperature. Single-phase growth is confirmed by XRD, epitaxially along the $\langle 012 \rangle$ direction for V_2O_3. After the transformation process, V_3O_5 and CdS become polycrystalline. Transport measurements were carried out on TTPX Lakeshore cryogenic probe station, using a Keithley 6221 current source and a Keithley 2182A nanovoltmeter. We used a Thorlabs LED with 400–700 nm wavelength range during the transport measurements.

All spin-polarized DFT[29,30] calculations were performed using the Vienna *Ab initio* Simulation Package (VASP)[29,31,32] within the projector augmented wave (PAW)[33] approach. The exchange-correlation effects were modeled using the Perdew–Burke–Ernzerhof (PBE)[34] generalized gradient approximations (GGA)[34] functional with a plane wave cutoff of 520 eV. The pseudopotentials used were similar to those used in the Materials Project,[35] where the core electrons were described with the frozen core approximation by the PAW potential, while the valence electrons of vanadium and oxygen are given by V:3p6 3d4 4s1 and O:2s2 2p4, respectively. The convergence criteria were set to 1×10^{-4} eV and -0.02 eV/Å for energies and atomic forces, respectively. The tetrahedron method with Blöchl corrections[36] was used for the insulating LT phase with Γ-centered k-point meshes of $1 \times 2 \times 2$ and $3 \times 4 \times 4$ for the relaxation of the supercells and for DOS calculations, respectively. All analysis and input generation were performed with the Python Materials Genomics (pymatgen) library.[37]

The initial V_3O_5 crystal structure with a space group P2/c was taken from Materials Project. The DFT + U method[38] was used for all calculations, with a Hubbard parameter U of 3.5 eV for V.[39] This U value resulted in a bandgap of 0.63 eV for LT V_3O_5, reproducing the experimental bandgap.[40] All calculations were performed in a ferromagnetic configuration.

All defect calculations were performed using $2 \times 2 \times 2$ (256 atoms) supercells of the conventional unit cell for the LT phase, which is large enough to minimize interactions between the periodic boundary images. We investigated neutral point defects focusing on vacancies and interstitials for both oxygen and vanadium. The vacancies were formed by removing one atom from the supercell and allowing the remaining atoms to relax. Interstitials were created by adding an atom at one of the ten symmetrically distinct sites found using Interstitially Finding Tool (InFiT).[41] More details of this method can be found in the work by Broberg *et al.*[42] Charged defects were studied by electron doping via the addition of integer numbers of electrons. It should be noted that VASP automatically adds a background compensating charge to achieve an overall charge neutral unit cell.

See the supplementary material related to the thermodynamic analysis and the structural characterization of the analyzed heterostructure.

The experimental investigation of coupled photoconducting and Mott materials was supported by the U.S. Air Force Office of Scientific Research under Award No. FA9550-20-1-0242. The theoretical aspects of this work were supported as part of the Quantum Materials for Energy Efficient Neuromorphic Computing (Q-MEEN-C), an Energy Frontier Research Center funded by the U.S. Department of Energy, Office of Science, Basic Energy Sciences, under Award No. DE-SC0019273. The authors also acknowledge computational resources provided by the Triton Shared Computing Cluster (TSCC) at the University of California San Diego. This research used resources of the National Energy Research Scientific Computing Center (NERSC), a U.S. Department of Energy Office of Science User Facility located at Lawrence Berkeley National Laboratory, operated under Contract No. DE-AC02-05CH11231.

AUTHOR DECLARATIONS

Conflict of Interest

The authors have no conflicts to disclose.

Author Contributions

Coline Adda: Formal analysis (equal); Investigation (equal); Methodology (equal); Writing – original draft (equal); Writing – review and editing (equal). **Henry Navarro:** Data curation (lead); Formal analysis (lead); Investigation (lead); Methodology (lead); Writing – original draft (lead); Writing – review and editing (equal). **Jasleen Kaur:** Resources (equal); Software (equal). **Min-Han Lee:** Investigation (equal); Resources (equal). **Chi Chen:** Resources (equal); Software (equal). **Marcelo J. Rozenberg:** Conceptualization (equal); Investigation (equal); Validation (equal); Writing – review and editing (equal). **Shyue Ping Ong:** Investigation (equal); Methodology (equal); Software (lead); Writing – original draft (equal); Writing – review and editing (equal). **Ivan K. Schuller:** Funding acquisition (equal); Investigation (equal); Resources (equal); Supervision (lead); Writing – original draft (equal); Writing – review and editing (lead).

DATA AVAILABILITY

The data that support the findings of this study are available from the corresponding authors upon reasonable request.

REFERENCES

[1] S. Larentis, F. Nardi, S. Balatti, D. C. Gilmer, and D. Ielmini, IEEE Trans. Electron Devices **59**(9), 2468–2475 (2012).
[2] S. Kim, S. Choi, and W. Lu, ACS Nano **8**(3), 2369–2376 (2014).
[3] Z. Wang, H. Wu, G. W. Burr, C. S. Hwang, K. L. Wang, Q. Xia, and J. J. Yang, Nat. Rev. Mater. **5**(3), 173–195 (2020).
[4] J. S. Lee, S. Lee, and T. W. Noh, Appl. Phys. Rev. **2**(3), 031303 (2015).
[5] Y. Li, Z. Wang, R. Midya, Q. Xia, and J. J. Yang, J. Phys. D **51**(50), 503002 (2018).
[6] R. Rocco, J. del Valle, H. Navarro, P. Salev, I. K. Schuller, and M. Rozenberg, Phys. Rev. Appl. **17**(2), 024028 (2022).
[7] D. Lelmini and R. Waser, *Resistive Switching: From Fundamentals of Nanoionic Redox Processes to Memristive Device Applications* (Wiley-VCH Verlag GmbH & Co. KGaA, 2016).
[8] N. F. Mott, Rev. Mod. Phys. **40**(4), 677–683 (1968).
[9] A. Zimmers, L. Aigouy, M. Mortier, A. Sharoni, S. Wang, K. G. West, J. G. Ramirez, and I. K. Schuller, Phys. Rev. Lett. **110**(5), 056601 (2013).

Published under an exclusive license by AIP Publishing

[10]S. Kumar, M. D. Pickett, J. P. Strachan, G. Gibson, Y. Nishi, and R. S. Williams, Adv. Mater. **25**(42), 6128–6132 (2013).
[11]S. Cheng, M.-H. Lee, X. Li, L. Fratino, F. Tesler, M.-G. Han, J. del Valle, R. C. Dynes, M. J. Rozenberg, I. K. Schuller, and Y. Zhu, Proc. Natl. Acad. Sci. U. S. A. **118**(9), e2013676118 (2021).
[12]S. Stathopoulos, I. Tzouvadaki, and T. Prodromakis, Sci. Rep. **10**(1), 21130 (2020).
[13]A. Kathalingam, H.-S. Kim, S.-D. Kim, and H.-C. Park, Opt. Mater. **48**, 190–197 (2015).
[14]B. Sun, Y. Liu, W. Zhao, and P. Chen, RSC Adv. **5**(18), 13513–13518 (2015).
[15]M. Ungureanu, R. Zazpe, F. Golmar, P. Stoliar, R. Llopis, F. Casanova, and L. E. Hueso, Adv. Mater. **24**(18), 2496–2500 (2012).
[16]X. Guan, W. Hu, M. A. Haque, N. Wei, Z. Liu, A. Chen, and T. Wu, Adv. Funct. Mater. **28**(3), 1704665 (2018).
[17]S. Sharma, A. Kumar, and D. Kaur, Appl. Phys. Lett. **115**(5), 052108 (2019).
[18]A. Mehonic, T. Gerard, and A. J. Kenyon, Appl. Phys. Lett. **111**(23), 233502 (2017).
[19]H.-K. He, R. Yang, W. Zhou, H.-M. Huang, J. Xiong, L. Gan, T.-Y. Zhai, and X. Guo, Small **14**(15), 1800079 (2018).
[20]H. Navarro, J. del Valle, Y. Kalcheim, N. M. Vargas, C. Adda, M.-H. Lee, P. Lapa, A. Rivera-Calzada, I. A. Zaluzhnyy, E. Qiu, O. Shpyrko, M. Rozenberg, A. Frano, and I. K. Schuller, Appl. Phys. Lett. **118**(14), 141901 (2021).
[21]S. Kose, F. Atay, V. Bilgin, I. Akyuz, and E. Ketenci, Appl. Surf. Sci. **256**(13), 4299–4303 (2010).
[22]C. Adda, M.-H. Lee, Y. Kalcheim, P. Salev, R. Rocco, N. M. Vargas, N. Ghazikhanian, C.-P. Li, G. Albright, M. Rozenberg, and I. K. Schuller, Phys. Rev. X **12**(1), 011025 (2022).
[23]N. Kumar, A. Rúa, J. Lu, F. Fernández, and S. Lysenko, Phys. Rev. Lett. **119**(5), 057602 (2017).
[24]V. N. Andreev and V. A. Klimov, Phys. Solid State **53**(12), 2424–2430 (2011).
[25]M.-H. Lee, Y. Kalcheim, J. del Valle, and I. K. Schuller, ACS Appl. Mater. Interfaces **13**(1), 887–896 (2021).
[26]A. Rúa, R. D. Díaz, N. Kumar, S. Lysenko, and F. E. Fernández, J. Appl. Phys. **121**(23), 235302 (2017).
[27]V. I. Kudinov, I. L. Chaplygin, A. I. Kirilyuk, N. M. Kreines, R. Laiho, E. Lähderanta, and C. Ayache, Phys. Rev. B **47**(14), 9017–9028 (1993).
[28]G. Nieva, E. Osquiguil, J. Guimpel, M. Maenhoudt, B. Wuyts, Y. Bruynseraede, M. B. Maple, and I. K. Schuller, Appl. Phys. Lett. **60**(17), 2159–2161 (1992).
[29]G. Kresse and J. Furthmüller, Phys. Rev. B **54**(16), 11169–11186 (1996).
[30]P. Hohenberg and W. Kohn, Phys. Rev. **136**(3B), B864–B871 (1964).
[31]G. Kresse and J. Hafner, Phys. Rev. B **47**(1), 558–561 (1993).
[32]G. Kresse and J. Furthmüller, Comput. Mater. Sci. **6**(1), 15–50 (1996).
[33]P. E. Blöchl, Phys. Rev. B **50**(24), 17953–17979 (1994).
[34]J. P. Perdew, K. Burke, and M. Ernzerhof, Phys. Rev. Lett. **77**(18), 3865–3868 (1996).
[35]A. Jain, S. P. Ong, G. Hautier, W. Chen, W. D. Richards, S. Dacek, S. Cholia, D. Gunter, D. Skinner, G. Ceder, and K. A. Persson, APL Mater. **1**(1), 011002 (2013).
[36]P. E. Blöchl, O. Jepsen, and O. K. Andersen, Phys. Rev. B **49**(23), 16223–16233 (1994).
[37]S. P. Ong, W. D. Richards, A. Jain, G. Hautier, M. Kocher, S. Cholia, D. Gunter, V. L. Chevrier, K. A. Persson, and G. Ceder, Comput. Mater. Sci. **68**, 314–319 (2013).
[38]V. I. Anisimov, J. Zaanen, and O. K. Andersen, Phys. Rev. B **44**(3), 943–954 (1991).
[39]B. Himmetoglu, A. Floris, S. de Gironcoli, and M. Cococcioni, Int. J. Quantum Chem. **114**(1), 14–49 (2014).
[40]N. J. Szymanski, Z. T. Y. Liu, T. Alderson, N. J. Podraza, P. Sarin, and S. V. Khare, Comput. Mater. Sci. **146**, 310–318 (2018).
[41]N. E. R. Zimmermann, M. K. Horton, A. Jain, and M. Haranczyk, Front. Mater. **4**, 34 (2017).
[42]D. Broberg, B. Medasani, N. E. R. Zimmermann, G. Yu, A. Canning, M. Haranczyk, M. Asta, and G. Hautier, Comput. Phys. Commun. **226**, 165–179 (2018).

Published under an exclusive license by AIP Publishing